Numerical simulation and experimental study of the extrusion process for rice straw powder based on EDEM

Chaoran Sun†, Wenke Ai†, Ping Jiang, Songlin Sun, Limei Chen, Shaohui Tan, Chongfeng Gao*

(*School of Mechanical and Electrical Engineering, Hunan Agricultural University, Changsha 410128, China*)

Abstract: The application of twin-screw extrusion technology in the field of straw pretreatment is constrained by the closed nature of its structure, and the internal material flow characteristics have yet to be fully elucidated. This has resulted in a paucity of scientific theoretical support for screw configuration design. To address this issue, this study employed the discrete element method (DEM) in conjunction with physical tests to calibrate the simulation model parameters of rice straw powder. The calibration results demonstrate that the discrepancy between the simulation stacking test and the physical test results is 3.68%, thereby indicating that the simulation model parameters are accurate and reliable. Subsequently, an extrusion verification comparison test of rice straw powder was conducted. The results demonstrated that the relative errors between the simulated and actual quality in different regions ranged from 7.95% to 12.45%. This evidence substantiates the applicability and reliability of the established simulation model in simulating the extrusion process of rice straw powder. Furthermore, the variation rules of the parameters of particle motion and their correlation during the extrusion process of rice straw powder were investigated. It was found that the filling degree was significantly correlated with other parameters, and that the screw configuration had a direct influence on the filling degree. Finally, a bench test was conducted to ascertain the viability of the established simulation model in guiding the design of screw configurations. A linear regression equation was derived between the simulated power consumption and the average particle size of extruded samples under different screw configurations. The study offers a particle-scale understanding of the visualization of the extrusion process of rice straw powder and the scientific design of screw configurations, which is of great significance for the industrial application of the extrusion method.

Keywords: rice straw, discrete element method, twin-screw extrusion, parameter calibration, numerical simulation

DOI: 10.25165/j.ijabe.20251802.9381

Citation: Sun C R, Ai W K, Jiang P, Sun S L, Chen L M, Tan S H, et al. Numerical simulation and experimental study of the extrusion process for rice straw powder based on EDEM. Int J Agric & Biol Eng, 2025; 18(2): 288–298.

1 Introduction

Straw is an abundant, green, and renewable resource that can be converted into high-value chemicals, fuels, and polymers through pretreatment, hydrolysis, and further processing[1,2]. However, the complexity of straw's structure and the diversity of its components limit the efficiency and effectiveness of subsequent processing[3,4]. Pretreatment is a crucial step in the utilization of straw resources, primarily encompassing chemical, physical, and enzymatic methods[5]. Twin-screw extrusion, as an emerging physical pretreatment technology, has garnered significant attention due to its high solid loading capacity, strong continuous processing capability, and excellent synergistic effects in composite treatments[6].

The principle of twin-screw extrusion technology involves the use of strong shear forces generated by the rotation of two co-rotating screws to disrupt the dense structure of straw, thereby enhancing the reaction rate of subsequent refining processes[7]. The screws are composed of various functional screw elements, typically classified into the conveying elements responsible for material mixing and transport, and kneading elements that provide strong tangential shear forces[8]. Kneading elements consist of multiple staggered kneading discs, and as the stagger angle increases, the function of the kneading elements transitions from strong distributive mixing to strong dispersive mixing. Strong dispersive mixing helps to break down the dense structure of straw, but its poor distributive mixing capability can lead to localized material accumulation, causing extrusion blockages and subsequent failures. Relevant studies have shown that screw configuration affects the flow state, stress conditions, and residence time of materials during the extrusion process, thereby influencing the effectiveness of straw extrusion pretreatment[9-12].

To investigate the patterns and mechanisms of material movement during the straw extrusion process, many scholars have conducted theoretical analyses and experimental studies. Meier et al.[13] explored the effects of different screw configurations on the sugar yield and biogas potential of wheat straw, using energy consumption, residence time, and temperature as indicators. The results showed that screw configuration significantly affects the residence time and absorbed shear energy during the extrusion process. Mundozah et al.[14] rationalized the positioning of various screw elements along the barrel by studying the particle size, particle porosity, liquid binder distribution, and residence time

Received date: 2024-09-22 **Accepted date:** 2025-02-13

Biographies: Chaoran Sun, PhD, Lecturer, research interest: innovative design of intelligent agricultural power platform, Email: scr@hunau.edu.cn; **Wenke Ai**, PhD candidate, research interest: agricultural mechanization engineering, Email: awk@stu.hunau.edu.cn; **Ping Jiang**, PhD, Professor, research interest: research on automation and intelligence technology and equipment of power machinery, Email: 1233032@hunau.edu.cn; **Songlin Sun**, PhD, Professor, research interest: innovative design and experimental research on agricultural power platform, Email: hnndssl@163.com; **Limei Chen**, PhD candidate, research interest: agricultural mechanization engineering, Email: lmchen0828@163.com; **Shaohui Tan**, PhD candidate, research interest: agricultural mechanization engineering, Email: tsh@stu.hunau.edu.cn.

†These authors contributed equally to this work.

***Corresponding author: Chongfeng Gao**, PhD, Lecturer, research interest: Technology and equipment of high value utilization of crop straw. School of Mechanical and Electrical Engineering, Hunan Agricultural University, Changsha 410128, China. Tel:+86-15201433675 , E-mail: gaocf@hunau.edu.cn.

distribution. They found that kneading elements increase the mixing degree of the material by enhancing particle stress in the tangential direction, while conveying elements facilitate material transport but are less effective for mixing. However, current research on straw extrusion pretreatment mainly relies on physical experiments, with limited involvement in numerical simulation studies. Therefore, employing convenient and efficient research methods to further expand the research means of straw extrusion pretreatment, achieving visualization and parameterization of the straw extrusion process, will help accelerate the industrialization of straw resource utilization.

DEM is a numerical simulation method based on the movement laws of microscopic particles, capable of simulating the movement and interaction of particles under complex flow and stress conditions, thereby revealing the macroscopic behavior and properties of particles[15-17]. The feasibility of using DEM to explore the “black box” model of extrusion has been reported. Li et al.[18] analyzed particle flow patterns, velocity fields, and screw motion during the extrusion process from a macroscopic point of view based on the DEM and found that the designed screw configuration could promote the cohesive flow of particles. Zheng et al.[19] studied the effect of particle shapes (sphere, cube, bilunabirotunda, and hexagonal prism) on the conveying characteristics of a twin-screw granulator using DEM. The results showed that the particle retention number, average residence time, and power consumption were minimized in the test group of spherical particles, and the flow pattern of spherical particles was closer to the ideal plug flow. Nevertheless, the majority of current DEM simulation studies on twin-screw extrusion are concentrated on polymer extrusion within the chemical industry, with comparatively limited research conducted on the extrusion process of straw within the agricultural sector. The crushing behavior of straw particles in a twin-screw pulping machine was simulated by Cheng et al.[20] using DEM, but a systematic and comprehensive understanding of how the screw elements affect the changes in internal material motion parameters and their interrelationships is still lacking. As a result, the design of the screw configurations still relies on numerous experiments, which severely restricts the industrialization process of straw extrusion pretreatment[21].

In light of the above, this paper proposes a simulation and experimental study of the rice straw powder extrusion process based on the DEM. Subsequently, the methodology of experimental design and correlation analysis was employed to elucidate the changing rules of the motion state parameters (filling degree, retention time, particle force, and motion speed) and the correlation relationship between the parameters of rice straw powder in the extrusion process. Then, the potential of the simulation model for guiding the screw combination design was investigated through bench tests. The study aims to achieve visualization and parameterization of the straw extrusion process and provide a scientific basis for screw configuration design in the extrusion process at the particle scale.

2 Materials and methods

2.1 Experimental materials

The experimental material used in this study was rice straw of the Denghai No.1 variety obtained from a farm in Muyang, Suqian, Jiangsu, China. The rice straw underwent natural air-drying before being cut to a length of 2-3 cm using a guillotine cutter. Following this, the straw was pulverized using a high-speed pulverizer (Ruihao, Zhejiang, China) through a 1 mm sieve to prepare the test samples. The moisture content of the rice straw powder was measured to be 10.4%±3.4% after continuous drying in an oven at 105°C for 10 h.

2.2 Experimental apparatus

The mechanical device implemented in this study was a custom-engineered 20-type twin-screw extruder. The technical specifications of the extruder include a barrel inner diameter (*D*) of 22.5 mm and a length-to-diameter ratio of 32.56. The screw components used in this study comprised conveyance and kneading elements, each with an outer diameter of 21.5 mm. The distance between the external diameter of the screw elements and the extruder barrel was maintained at 1 mm.

2.3 Calibration of simulation model parameters

2.3.1 Physical experiment on the angle of repose of rice straw powder

Referring to the national standard GB/T 16913.5-1997 and related literature[22], a funnel method was used to conduct a physical experiment on the angle of repose with a fixed mass of material. The prepared rice straw powder was slowly poured into a funnel, allowing the material to fall uniformly and form a heap. The stainless steel funnel had a top disc diameter of 170 mm, a cone angle of 45°, an outlet diameter of 22 mm, and a distance of 100 mm between the outlet and the upper surface of the steel plate. The rice straw powder was slowly poured into the funnel until the angle of repose of the material on the bottom steel plate no longer changed. The original image of the angle of repose was captured (Figure 1a) and processed using Python-OpenCV software (OpenCV Foundation, USA) (Figure 1b). The edge contour coordinates were extracted and linearly fitted (Figure 1c) to calculate the slope of the fitted line and the average angle of repose. The experiment was repeated 15 times, yielding an average physical angle of repose for the rice straw powder of 30.96° with a coefficient of variation of 4.3%.

a. Straw powder pile b. Binarized image c. Edge coordinate extraction

Figure 1 Angle of repose processing image

2.3.2 Simulation experiment on the angle of repose of rice straw powder

Due to the adhesion phenomenon between particles during the extrusion process of rice straw powder, the Hertz Mindlin with JKR Cohesion contact model, which is a cohesive particle contact model based on Hertz theory, was selected for the equivalent calibration of contact parameters for rice straw powder. This model is suitable for powder particles such as pharmaceuticals, as well as materials like crops, ores, and soil.

In the simulation model, the internal geometric dimensions of the barrel, the types, quantities, and positions of screw elements were consistent with the actual experiments. To improve the simulation efficiency without compromising the model's reliability, the team, based on preliminary experiments and literature reviews, selected 1 mm diameter microspheres to replace the rice straw powder particles[22]. Based on domestic and international literature on the setting of discrete element simulation parameters for powder particles and steel plates[23,24], the simulation parameter range for rice straw powder was determined, as listed in Table 1.

Table 1 Simulation parameters of rice straw powder particle accumulation angle

Parameter	Value
Rice straw powder density/(kg·m^{-3})	573.9
Rice straw powder Poisson's ratio	0.4
Rice straw powder shear modulus/Pa	1×10^6
Steel plate density/(kg·m^{-3})	7850
Steel plate Poisson's ratio	0.3
Steel plate shear modulus/Pa	7×10^{10}
Powder-powder restitution coefficient X_1	0.15-0.30
Powder-powder static friction factor X_2	0.40-0.80
Powder-powder rolling friction factor X_3	0.10-0.30
Powder-steel restitution coefficient X_4	0.15-0.30
Powder-steel static friction factor X_5	0.30-0.70
Powder-steel rolling friction factor X_6	0.05-0.15
JKR surface energy X_7/(J·m^{-2})	0.001-0.002

2.4 Simulation analysis of the extrusion process of rice straw powder

To investigate the feasibility of using the discrete element method for simulating the rice straw extrusion process, extrusion validation tests were conducted using the quality of straw powder from different regions as an indicator. Material motion changes primarily occur in the kneading element region and affect the material movement in the front-end conveying region[25]. Therefore, six calculation zones were selected as shown in Figure 2, with Zone 3 and Zone 6 being kneading elements, and the remaining zones being conveying elements.

Under laboratory conditions, the screw speed is usually between 30 and 120 r/min[26]. To ensure the comparability of the experimental data, this paper set up the twin-screw extruder at a medium screw speed (60 r/min) for the test, with a feeding rate of 10 g/min and a total extrusion time of 40 s. The quality of the rice straw powder in the different zones was measured and recorded at the intervals of 5 s, starting from the feeding instant.

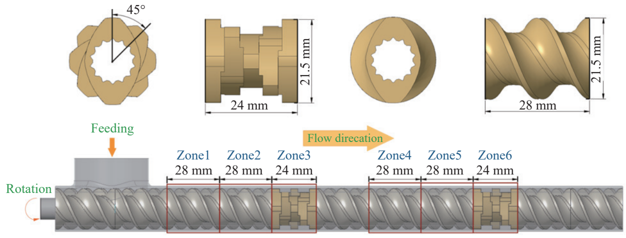

Figure 2 Schematic diagram of computational domain division

A geometric model of the extrusion device was established in Creo 3D software and converted into STP format for import into DEM software. The particle parameters of the simulation model were set according to the parameters calibrated earlier, and the screw speed, feeding rate, screw configuration, and measurement intervals were consistent with the physical experiment settings.

2.5 Comparative simulation experiments of extrusion with different screw configurations

Twin-screw extrusion is a physical pretreatment method that primarily disrupts the dense structure of straw through mechanical kneading at the kneading element. To explore the feasibility of using the simulation model for guiding the design of different screw configurations, the K90 kneading element, which solely has a kneading function, was chosen as the test object. The number of screws was used as a test variable, and indices such as simulated energy consumption, actual energy consumption, and average particle size were employed to conduct extrusion simulation and comparison tests under different screw configurations. Different screw configurations were modeled in 3D using Creo 7.0, as shown in Figure 3, and imported into EDEM software in STP format for simulation experiments. The different experimental groups were labeled as K90-x (where x represents the number of kneading elements). Particle size distribution was measured using a MASTERSIZER 3000 laser particle size analyzer (Malvern, UK), with each sample tested three times. The extrusion control parameters for both simulation and physical experiments were consistent with those in section 2.4.

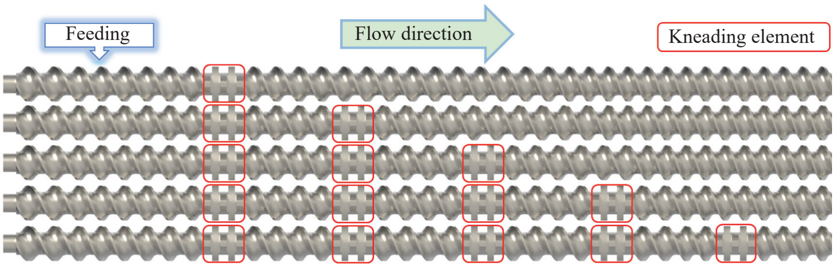

Figure 3 Configuration of screws

3 Results and analysis

3.1 Calibration results and analysis of the simulation model parameters for rice straw powder

To identify the parameters that significantly affect the angle of repose of rice straw powder, simulation stacking experiments were conducted based on the Plackett-Burman experimental design principle, using the parameter ranges of X_1 to X_7 listed in Table 1. The experimental results and variance analysis are presented in Tables 2 and 3.

As listed in Table 2, the simulation experiments on the angle of repose within the selected parameter range resulted in angles between 25.36° and 33.21°, with the physical angle of repose falling within this range. Table 3 indicates that parameters X_1 and X_5 have a highly significant effect on the simulated angle of repose (p<0.01), while X_7 has a significant effect (p<0.05). The remaining parameters do not significantly affect the angle of repose of rice straw powder (p>0.05).

Table 2 Plackett-Burman experimental results

No.	X_1	X_2	X_3	X_4	X_5	X_6	X_7	Stacking angle/(°)
1	–1	–1	+1	–1	+1	+1	–1	29.74
2	+1	+1	–1	+1	+1	+1	–1	30.76
3	+1	+1	–1	–1	–1	+1	–1	28.77
4	+1	–1	+1	+1	+1	–1	–1	32.67
5	–1	–1	–1	–1	–1	–1	–1	25.36
6	–1	–1	–1	+1	–1	+1	+1	27.10
7	+1	–1	+1	+1	–1	+1	+1	31.13
8	–1	+1	–1	+1	+1	–1	+1	29.77
9	+1	–1	–1	–1	+1	–1	+1	33.21
10	+1	+1	+1	–1	–1	–1	+1	30.14
11	–1	+1	+1	–1	+1	+1	+1	29.76
12	–1	+1	+1	+1	–1	–1	–1	26.06

Table 3 Analysis of parameters of significance

Parameter	Standardization effect	Mean sum of square	F value	p value	Significance ranking
X_1	3.148	29.7400	112.8200	0.0004	1
X_2	–0.658	1.3000	4.9300	0.0905	5
X_3	0.755	1.7100	6.4900	0.0635	4
X_4	0.085	0.0217	0.0800	0.7885	6
X_5	2.891	25.0900	95.1700	0.0006	2
X_6	0.008	0.0002	0.0008	0.9789	7
X_7	1.291	5.0100	18.9900	0.0121	3

Therefore, in subsequent response surface experiments, only the parameters X_1, X_5, and X_7 were considered, with the other parameters set to their mid-level values. The coding table of response surface experiment factors and the experimental results are listed in Tables 4 and 5, respectively. The variance analysis of the Box-Behnken experimental results is presented in Table 6.

Table 4 Box-Behnken test coding table

Level	Factors		
	X_1	X_5	X_7
–1	0.150	0.30	0.0010
0	0.225	0.50	0.0015
1	0.300	0.70	0.0020

As listed in Table 5, the response surface experiments conducted within the selected parameter range resulted in simulated angles of repose between 26.72° and 33.94°. Table 6 shows that the model fit is highly significant (p<0.01); X_1, X_5, X_1^2, and X_5^2 all have highly significant effects on the simulated angle of repose of rice straw powder (p<0.01). By optimizing the fitted equation, a quadratic regression equation model between the significant parameters and the angle of repose θ was obtained, as shown in Equation (1):

$$\theta = 0.87 + 115.96X_1 + 46.07X_5 + 1392.50X_7 - 207.46X_1^2 - 36.24X_5^2 \tag{1}$$

Using the physical angle of repose of rice straw powder as the target value, the regression equation was optimized in the post-processing module of Design-Expert 13, resulting in the optimal values of the parameters: collision restitution coefficient X_1 of 0.213, static friction coefficient between straw powder and steel plate X_5 of 0.414, and JKR surface energy X_7 of 0.001 J/m^2. The five sets of simulation stacking tests were repeated under the parameters of the optimal solution, and the average value of the simulation stacking angle was obtained, resulting in a value of 29.82° and a relative error of only 3.68% in comparison to the physical stacking angle. The results demonstrate that the calibrated parameters are accurate and reliable, and can be employed for the discrete element simulation of rice straw flour. A comparison of the simulation stacking test result with the physical stacking test result is presented in Figure 4.

Table 5 Test and results of Box-Behnken

No.	X_1	X_5	X_7	Stacking angle/(°)
1	–1	–1	0	26.72
2	–1	0	1	30.54
3	0	0	0	33.13
4	1	1	0	33.65
5	0	0	0	32.30
6	1	–1	0	30.27
7	0	–1	–1	27.89
8	0	0	0	32.17
9	0	1	1	33.94
10	–1	0	–1	28.78
11	0	–1	1	29.22
12	0	1	–1	33.36
13	–1	1	0	29.71
14	1	0	1	33.23
15	0	0	0	32.81
16	0	0	0	32.93
17	1	0	–1	33.53

Table 6 Anova of Box-Behnken quadratic regression model

Source	Sum of squares	Mean square	F value	p value
Model	80.1300	8.9000	24.5800	0.0002
X_1	27.8600	27.8600	76.9300	<0.0001
X_5	34.2800	34.2800	94.6400	<0.0001
X_7	1.4200	1.4200	3.9200	0.0882
$X_1 X_5$	0.0380	0.0380	0.1050	0.7554
$X_1 X_7$	1.0600	1.0600	2.9300	0.1307
$X_5 X_7$	0.1406	0.1406	0.3883	0.5530
X_1^2	4.9200	4.9200	13.6000	0.0078
X_5^2	9.4600	9.4600	26.1200	0.0014
X_7^2	0.0186	0.0186	0.0514	0.8271
Residual	2.5400	0.3622	-	-
Lack of fit	1.85	0.6166	3.60	0.1241
Pure error	0.6857	0.1714		
Cor total	82.67			
R^2=0.964; R^2_{adj}=0.948; CV=2.44%; R_{Pred}=0.907				

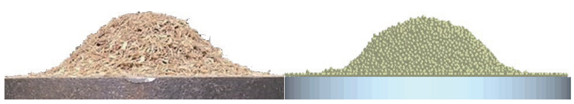

a. Physical experiment result b. Simulation results

Figure 4 Comparison of physical experiment and simulation results

3.2 Simulation results and analysis of rice straw powder extrusion

3.2.1 Results of extrusion validation comparison experiments

The comparison between the simulation result and the physical experiment result of rice straw powder extrusion is shown in Figure 5. The changes in particle mass over time in different regions for the simulation experiments and the physical experiment samples are illustrated in Figure 6.

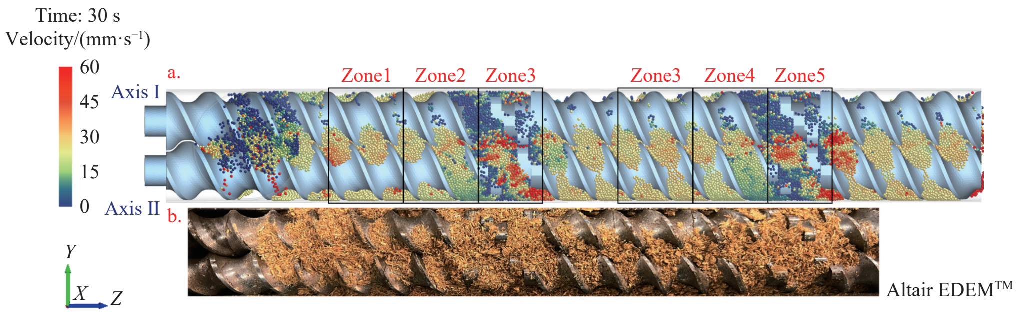

Note: a. Simulated particle distribution; b. Rice straw powder distribution

Figure 5 Comparison between simulation and actual results

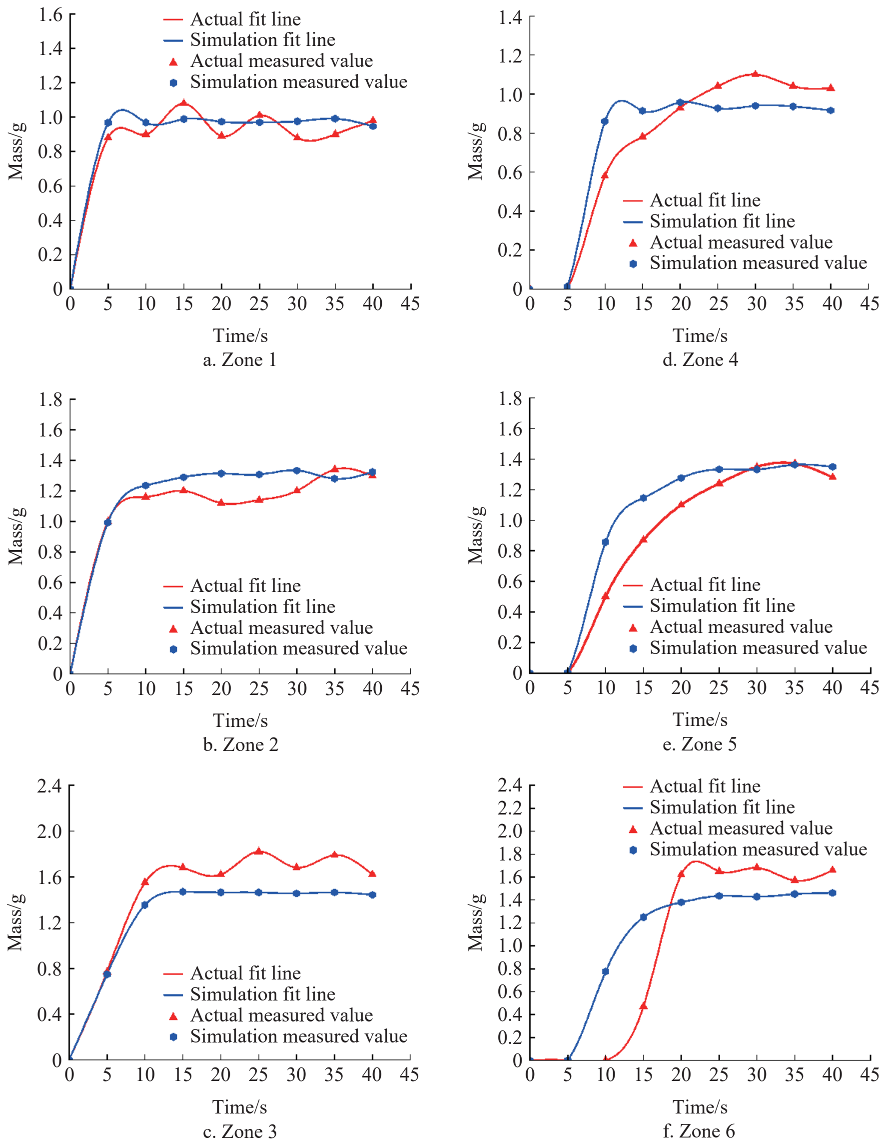

Figure 6 Variation of particle mass in different zones over time during simulation experiment and physical experiment

Figure 5 shows that the material distribution patterns of the simulation and physical tests are very similar when the extrusion process reaches stability. The material is more concentrated in the kneading area, whereas in the conveying area, it is mainly concentrated on the side of shaft II and the middle area of the two shafts. The masses of the material in Zones 2 and 3 are enhanced compared with Zone 1, and are 1.42 and 1.83 times higher, respectively, when stabilized. Furthermore, observed from Figure 5b, the material in the kneading region exhibits a certain degree of slate phenomenon during the physical test. This is consistent with the phenomena observed by Said et al.[27]

As shown in Figure 6, the simulation and physical experiment results for the six selected regions both exhibit an initial increase followed by stabilization. Once the extrusion process reaches a steady state, the relative error between the simulated and actual mass in different regions ranges from 7.95% to 12.45%.

Specifically, the relative error between the simulation results and physical experiment results is smallest for Zone 1 and Zone 2 (Figure 6a and 6b). Due to the retention effect of Zone 3 on the material, the particle mass in Zone 2 is higher than in Zone 1 when stable. The physical experiment results for Zone 3 are significantly higher than the simulation results after stabilization. This discrepancy arises because, during the actual extrusion process, the rice straw powder undergoes significant physical changes under the strong shear force of the kneading elements, causing some powder to agglomerate, thereby altering its density and bulk density within the barrel. In contrast, the rigid particles in the simulation do not undergo volume shrinkage or mass changes, resulting in slightly lower simulated values compared to the actual measurements after stabilization (Figure 6c).

Before reaching a steady state, the relative error between the simulation and actual values is larger for Zone 4, Zone 5, and Zone 6, due to the retention effect of Zone 3 affecting the particle flow patterns in subsequent regions. The simulation values for Zone 4 stabilize around 15 seconds, while the actual values stabilize at 25 seconds (Figure 6d). Analysis indicates that the actual values for Zone 3 stabilize around 15 seconds, and the growth rate of the actual values for Zone 4 significantly slows at 15 seconds. This suggests that the increase in material mass in Zone 4 after 15 seconds is primarily due to the retention effect of particles in Zone 6, transmitted through Zone 5. Additionally, the more pronounced retention effect of material in Zone 3 during actual operation causes the actual values for Zone 4 to stabilize approximately 10 seconds later than the simulation values. The stabilization process for Zone 5 is slower, with the simulation and actual values stabilizing around 23 seconds and 25 seconds, respectively (Figure 6e). The growth trends of the simulation values for Zone 5 and Zone 6 are very similar, indicating that the increase in simulated particle mass in Zone 5 may be influenced by Zone 6 (Figure 6f). The relative error between the stabilized simulation and actual values for Zone 6 is similar to that of Zone 3.

In summary, after reaching a steady state, the errors between the simulation and physical experiments in different regions are relatively small, indicating that the established model can be used to simulate the extrusion process of rice straw powder.

3.2.2 Analysis of filling level

The filling level, a critical indicator that reflects the internal pressure within an extruder[28], is defined as the ratio of the particle count, N_t, within a specific region at different time points to the particle count, N_T, corresponding to the region's saturated state. Figure7 depicts the variation of particle count and filling level across different regions over time, obtained by conducting a 40 s simulation in the EDEM. The relationship between the filling level (φ_n) and the particle count (N) in different regions can be expressed as:

$$\varphi_n = \frac{N_t}{N_T} \tag{2}$$

where, N_t denotes the number of particles in the region at a certain point in time, N_T denotes the number of particles in the region when the number of particles reaches saturation, and n is the region number.

Figure 7a shows that the number of particles in all zones gradually stabilizes with small fluctuations over time. The conveying zone experiences considerably smaller fluctuations than the kneading zone. After reaching stability, the average number of simulated particles in Zones 1-6 are 3233, 4331, 4854, 3125, 4455, and 4874, respectively. Figure 7b shows that Zone 1 reaches the stable process faster than other zones, with a filling level after stabilization of 33.6%, indicating that the filling level of this zone is mainly related to the feeding speed. Zone 2 reaches the stable state in a considerably longer time than Zone 1, but slightly shorter than Zone 3. The curve shape of Zone 2 before reaching stability is very similar to that of Zone 3. After stabilization, the filling level of Zone 2 was 45.01%, which was higher than the 33.94% in Zone 1. This phenomenon shows that the filling level of Zone 2 is strongly influenced by Zone 3. Zone 3 tends to stabilize at 13 s, and its filling level after stabilization is 88.22%. The filling level of Zone 4 after reaching stabilization is almost the same as that of Zone 1, and the filling level of Zone 5 is the same as that of Zone 6. After stabilization, the filling levels of Zones 1, 2, and 3 are approximately equal to the filling levels of Zones 4, 5, and 6, respectively. The time taken for Zones 1-3 to reach a stable state is considerably shorter than that of Zones 4-6. This may be due to the retention effect of Zone 3 on the simulated particles, altering the original axial conveying efficiency and reducing the number of particles entering the subsequent zone. Therefore, the filling level at Zone 5 is affected by the extrusion speed of particles at Zone 3 and the retention effect of particles at Zone 6.

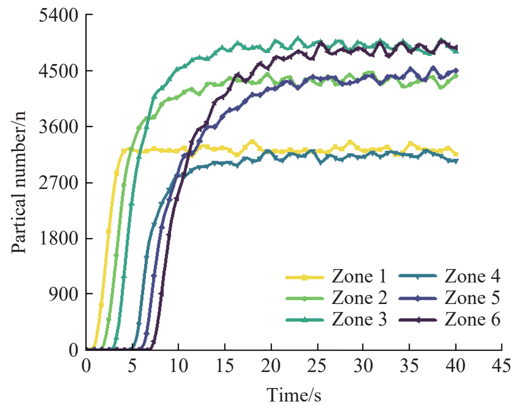

a. Particle number

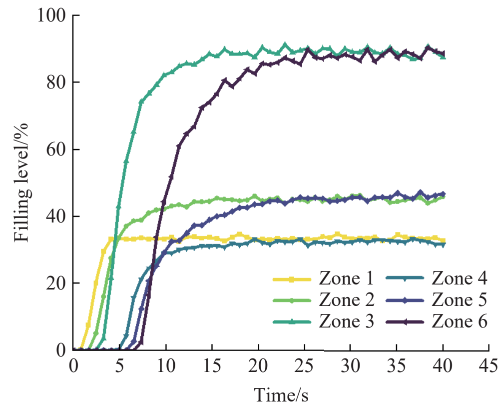

b. Filling level

Figure 7 Variation of particle number and filling level in different regions over time

3.2.3 Analysis of average retention time

To explore the retention effects of simulated particles in different regions at various stages and their temporal variations, the extrusion process was divided into three phases: the initial stage (0-10 s), the filling stage (10–30 s), and the stable stage (after 30 s). At time points of 0 s, 10 s, 20 s, and 30 s, five simulated particles were randomly selected, and their displacement along the Z-axis (denoted as L) was recorded as a function of simulation time (t). The residence effect (ψ) was calculated, defined as the time required for a particle to traverse a unit distance along the Z-axis:

$$\psi = \frac{\mathrm{d}t}{\mathrm{d}L} \tag{3}$$

At the initial stage, the simulated particle's axial motion velocity in Zone 1 is denoted as v_0. The time taken by simulated particle i to pass through region n is represented as t_{in}, and L_n represents the axial length of region n. The average retention time T_n for particles within region n satisfies:

$$T_n = \frac{\sum_{i=1}^{5}\left(t_{\mathrm{in}} - \frac{L_n}{v_0}\right)}{5} \tag{4}$$

Figure 8 shows that the conveying region has almost no retention effect on the simulated particles during different filling periods. However, the simulated particles in the kneading region exhibit complex motion characteristics, such as acceleration, deceleration, and backflow. In the initial stage (Figure 8a), the motion of the simulated particles, as they traverse through the kneading region, maintains relative stability, with an average retention time of 11.18 s. The presence of a singular kneading element augments the average retention time of the simulated particles by 0.44 s. During the 10 s filling stage (Figure 8b), the trajectory of the simulated particles as they enter the extruder barrel exhibits a trend analogous to that seen in the initial stage, characterized by relatively consistent motion. However, upon reaching the 20 s mark, certain particles undergo alterations in their positional and temporal trends. At this juncture, the average retention time of the particles is 13.71 s, with a singular kneading element contributing a 0.62 s increase to the average retention time of the simulated particles. In the 20 s filling stage (Figure 8c), particles manifest substantial alterations post-traversing the first kneading element, and these alterations intensify after they pass through the second kneading element. At this stage, the average retention time of the particles is 12.13 s, with a single kneading element augmenting the average retention time of the simulated particles by 0.66 s. In the stable 30 s stage (Figure 8d), simulated particles entering the extruder barrel display substantial changes in their motion within the first conveying element region when compared with the other stages. At this point, the retention effect of Zone 3 on simulated particles reaches its zenith, with a singular kneading element contributing a 0.97 s increase to the average retention time of the simulated particles. It can be observed that the retention effect of the material in the kneading zone reaches its maximum when stable, and increasing the retention time of the material helps to achieve better straw pretreatment results[29].

3.2.4 Analysis of motion velocity

The particle velocities along different directions and the changes in the particle distribution state with time were analyzed to investigate the flow characteristics of rice straw powder inside the extruder barrel. As shown in Figure 9, the average velocities V_x, V_y, and V_z of simulated particles along different directions in different regions during filling were measured and plotted against time. The variation of the simulated particle distribution with time is shown in Figure 10.

Figure 9 shows substantial differences in the velocity components of particles across different zones in the X-, Y-, and Z-axis directions. The velocity ranges were −2.41-2.00 mm/s,−0.43-2.24 mm/s, and 14.37-26.05 mm/s, respectively. Zones 4 and 5 had higher average velocities than Zones 1 and 2, respectively, in the X-axis direction, while their velocities were similar in the Y-axis direction. As observed in Figure 10, the particles are collected on the side of axis II after passing through Zone 3, increasing the density difference of the particles in the X-axis direction, which accelerates the velocity of the particles in the X-axis direction, while

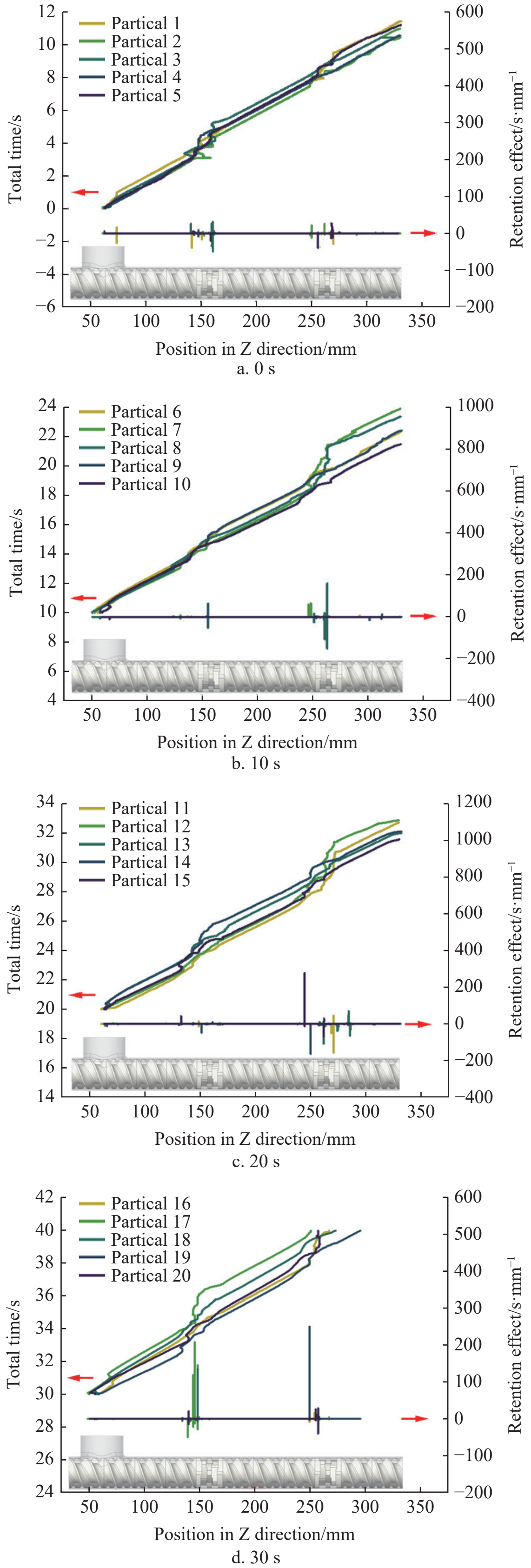

Figure 8 Displacement-time relationship of particles entering the barrel at different times

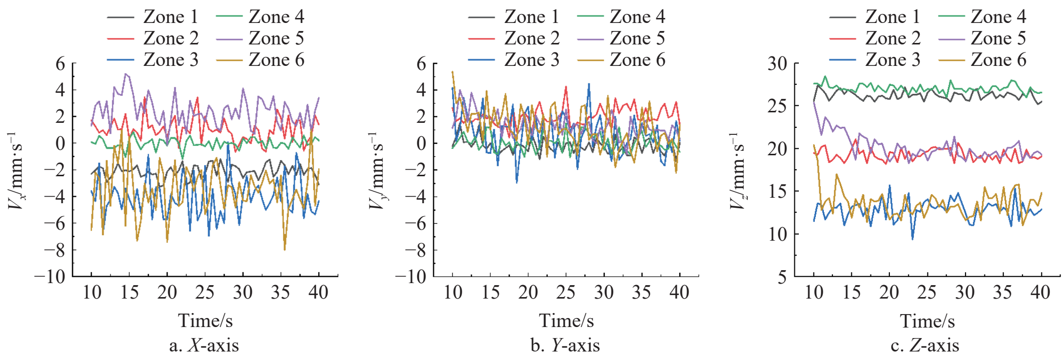

Figure 9 Variation of simulated particle velocity along different directions

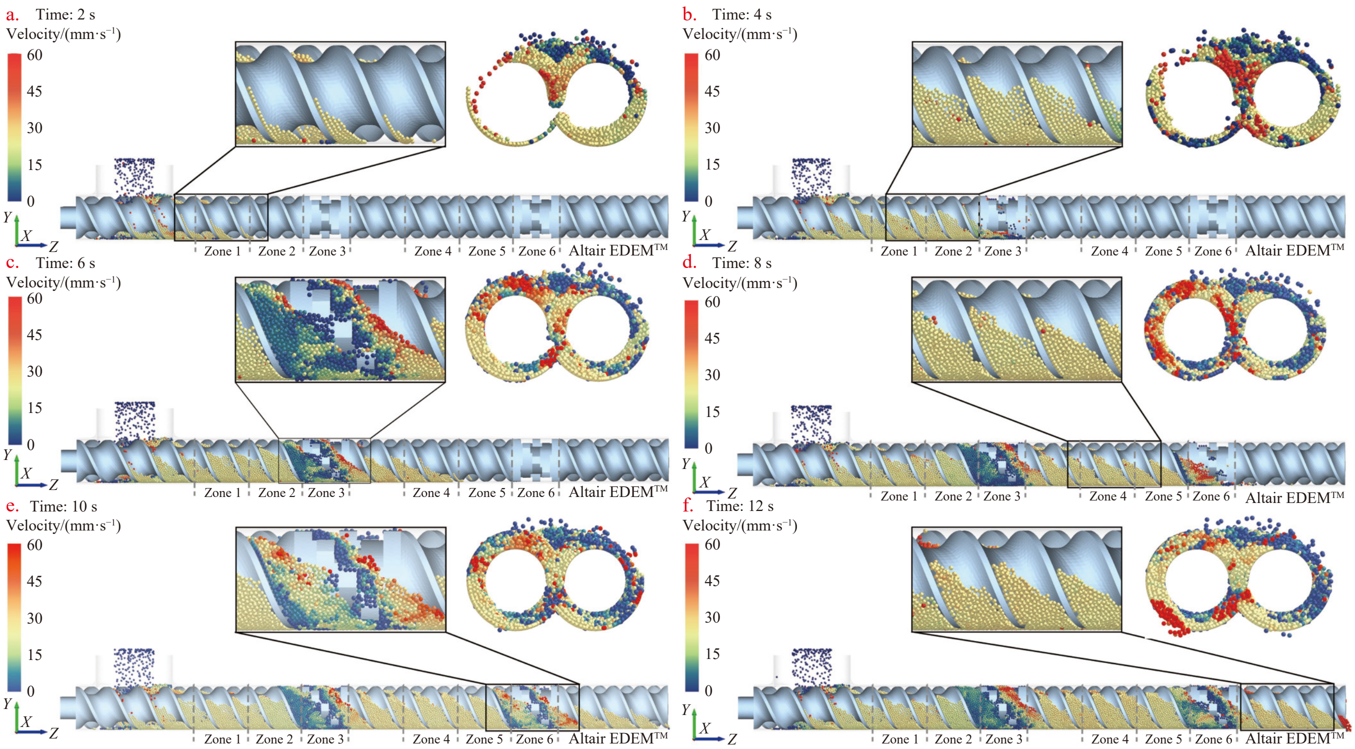

Note: a: 2 s, b: 4 s, c: 6 s, d: 8 s, e: 10 s, f: 12 s

Figure 10 Simulated particle distribution at different time points

the velocity component in the *Y*-axis is relatively stable. As observed, a clear stratification of particle velocities in different regions along the *Z*-axis exists, which may be attributed to varying filling levels in these regions, as shown in Figure 7b.

3.2.5 Analysis of the particle forces

To determine the change rule of force on simulated particles during the extrusion process, the force on simulated particles in different zones along different directions during the filling period was measured. The results are plotted over time, as shown in Figure 11. Once the extrusion process reached stability, the force on simulated particles in Zones 2 and 3 was analyzed, as shown in Figure 12. The direction of simulated particle motion is illustrated in Figure 13.

As shown in Figure 11, the symmetrical structure of the twin screw results in the simulated particles being subjected to forces F_x and F_y of very similar magnitude in the *X*- and *Y*-axis directions. In addition, the variation of the force on the particles in different regions of the same direction is very substantial. Specifically, Zones 1 and 4 have a very small force magnitude in all directions, averaging at 2.30×10^{-7} N. Zones 2 and 5 have a similar force magnitude, which is higher than that of Zones 1 and 4, averaging at 1.65×10^{-6} N. Zones 3 and 6 have a much larger force magnitude in the *X*-axis and *Y*-axis, averaging at 2.67×10^{-5} N, and a smaller force magnitude in the *Z*-axis, averaging at 7.18×10^{-6} N.

Figure 12 shows that when the extrusion process reaches stability, the total force on the simulated particles in the selected region shows a periodic variation. At 30.0 s, the simulated particles are conveyed axially under the influence of the conveying element, with a relatively small total force. Between 30.1 s and 30.3 s, the simulated particles in the conveying region converge with those trapped in the kneading region due to the axial action of the conveying element. This phenomenon increases the local filling level and subsequently, the interaction force between the particles. At 30.4 s, the majority of the simulated particles enter the meshing region, further increasing the filling level of the region. The particles are subjected to strong shear forces exerted by the kneading elements in the tangential direction, which helps disrupt the cellulose structure[30]. At 30.5 s, all simulated particles migrate to the kneading region and their force state is consistent with that observed at 30.0 s. The regions where particles are subjected to forces can be primarily divided into two categories: firstly, the interface between the conveying zone and the kneading zone, where particles experience both the axial force from the conveying element and the tangential shear force from the kneading element; secondly, the area between different kneading discs within the kneading zone, where particles are subjected to intense tangential shear forces. Consequently, these two regions exhibit more pronounced physical wear.

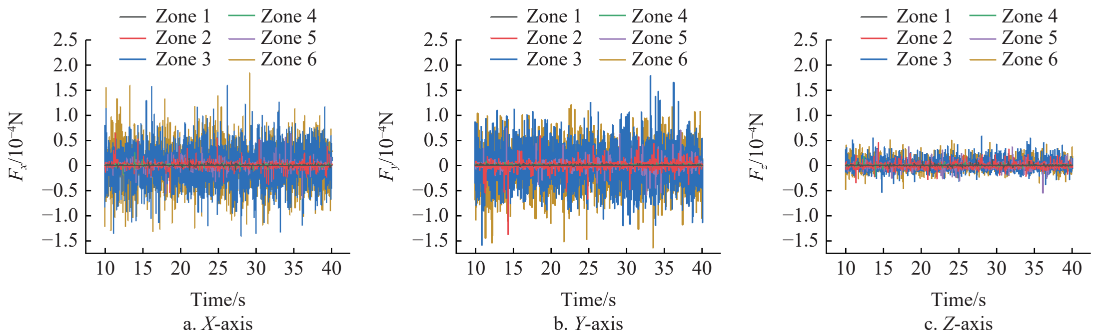

Figure 11 Variation of simulated particle forces along different directions

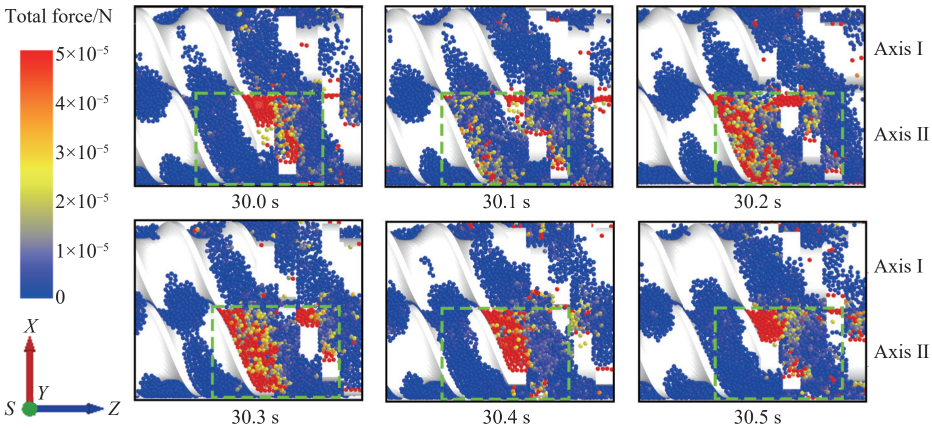

Figure 12 Variation of force with time for simulated particles of Zones 1 and 3

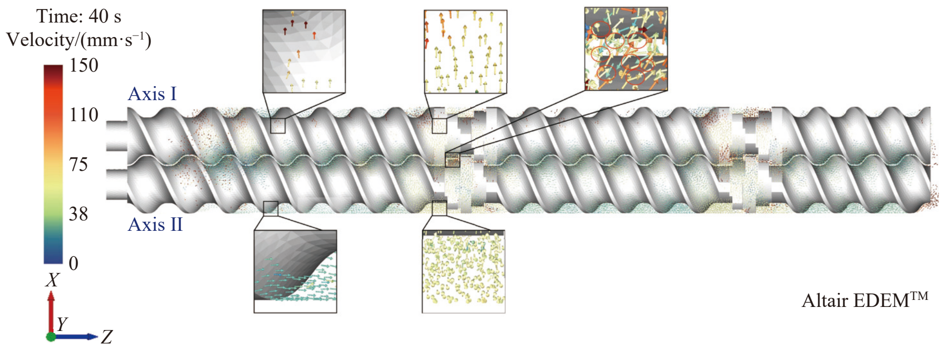

Figure 13 Direction of motion of simulated particles at 40 s

The results show that the magnitude of the force on the particles is closely related to the region they are located. The force on the particles in the conveying region is small in all directions, but increases as the distance from the kneading region decreases. The particles in the kneading region are subjected to a strong shear force, occurring periodically at the tips of the various kneading discs. This periodic force creates a periodic local pressure difference in the kneading region, resulting in the three phenomena of acceleration, retention, and backflow of the particles, as shown in Figure 13.

3.2.6 Correlation analysis

To investigate the motion state parameters of the simulated particles during the twin-screw extrusion process and the correlation between these parameters, the study commenced at the filling stage with five simulated particles randomly selected every 10 s. The parameters recorded as the particles passed through Zones 1 to 6 included the filling level (φ_n), average residence time (T_n), motion velocities (V_x, V_y, and V_z), and forces (F_x, F_y, and F_z). These parameters were then subjected to a correlation analysis as shown in Figure 14.

According to Figure 14, ϕ_n has a highly substantial positive correlation with T_n, $F_{x,y,z}$, and $V_{x,y}$ ($0.2\leq|r|<0.6$, $p<0.01$) and a considerably negative correlation with V_z ($|r|\geq0.8$, $p<0.01$). This result shows that the filling level is an important factor in the evaluation and development of extrusion pretreatment processes, as all other parameters related to filling level showed a highly substantial correlation[31]. There was no substantial correlation between T_n and $F_{x,y,z}$ or $V_{x,y}$ ($r<0.2$, $p>0.05$). However, a highly substantial negative correlation between T_n and V_z ($0.4\leq|r|<0.6$, $p>0.05$) exists, suggesting that the T_n of the particle flow is mainly influenced by V_z rather than the applied forces or tangential velocities. A substantial negative correlation was found between V_z and $F_{x,y,z}$ ($0.2<|r|<1$, $p<0.05$). This correlation may be attributed to the intensification of particle motion caused by the strong shear force applied in the kneading region. Furthermore, the strong shear forces exerted by different kneading discs in the kneading zone exhibit a certain periodicity. The application of these periodic forces creates periodic local pressure differences[32]. Under the influence of this pressure difference, the motion of the particles becomes chaotic, resulting in simultaneous acceleration, deceleration, and backflow of motion. A substantial negative correlation ($0.2<|r|<0.6$, $p>0.05$) is observed between V_z and $V_{x,y}$, whereas no correlation exists between $V_{x,y}$ and $F_{x,y}$. This lack of correlation may be due to the symmetric structural properties of the twin screw. A substantial positive correlation ($r>0.8$, $p<0.01$) exists between F_x and F_y, which are considerably correlated with F_z. This result suggests a correlation between axial and tangential forces on particles. The kneading element likely causes an increase in the local filling level when applying an improved shear force, intensifying the interaction between the particles[31]. Thus, the axial movement of particles in the kneading region is primarily caused by the formation of a pressure gradient, resulting in particle flow from the high-pressure region to the low-pressure region[33].

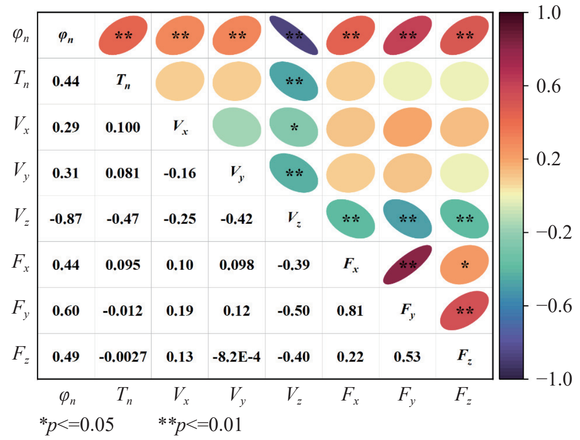

Figure 14 Correlation analysis between different parameters

3.3 Simulation comparative test results and analysis of different screw configurations

The simulation comparative test results under different screw configurations are listed in Table 7. The correlation analysis of the test results is presented in Table 8.

Table 7 Simulation results for different screw configurations

No.	Combination type	Physical results		Simulation results
		A: Actual power consumption/W	B: Average particle size/mm	C: Simulated power consumption/W
1	k90-1	39.46	0.4010	31.19
2	k90-2	51.68	0.3845	37.77
3	k90-3	71.45	0.3715	40.07
4	k90-4	83.38	0.3230	42.14
5	k90-5	92.06	0.3080	50.48

From Table 7, it is evident that with the increment of kneading elements, the actual extrusion power consumption escalates from 39.46 W to 92.06 W, while the average particle size of the material diminishes from 0.401 mm to 0.308 mm. This trend suggests that an increase in the number of kneading elements induces higher extrusion power consumption, which is beneficial for achieving superior extrusion crushing effects.

Table 8 Correlation analysis results

Index	A: Actual power consumption/W	B: Average particle size/mm	C: Simulated power consumption/W
Actual power consumption	1	-	-
Average particle size	–0.956 03*	1	-
Simulated power consumption	0.937 48*	–0.919 16*	1

Note: * indicates a significant correlation at the $p<0.05$ level.

As evidenced in Table 8, there is a markedly positive correlation between the actual and simulated power consumption ($r>0.8$, $p<0.05$), and a similarly significant negative correlation between both variables and the average particle size ($r<–0.8$, $p<0.05$).

However, the relative error between the two progressively enlarges, aligning with the analysis presented in section 3.2.1.

Correlation analysis results indicate a robust positive correlation between actual power consumption and simulated power consumption ($r>0.8$, $p<0.05$), and a significant negative correlation between both actual and simulated power consumption and average particle size ($r<–0.8$, $p<0.05$). The relationships among actual power consumption (A), average particle size (B), and simulated power consumption (C) can be mathematically represented as follows:

$$B = -0.0012A + 0.454 \tag{5}$$

$$C = 0.223A + 22.91 \tag{6}$$

$$C = -27.35B + 51.57 \tag{7}$$

In conclusion, the simulation model developed in this study demonstrates significant applicability in predicting power consumption and particle size. It serves as a valuable tool for guiding the design of screw configurations, providing effective references for optimizing energy consumption and controlling particle size in practical production processes.

4 Conclusions

In this study, the DEM combined with physical tests was used to carry out the simulation and experimental study of the extrusion process of rice straw powder, and the main work and conclusions are as follows:

1) The simulation model parameters of rice straw powder were calibrated by stacking angle simulation validation test. The results show that the relative error between the stacking angle simulation and the experimental results is 3.68%, indicating that the calibrated parameters are suitable for the discrete element simulation of rice straw powder.

2) The simulation tests of rice straw powder extrusion using calibrated parameters showed that the relative errors between the simulated and actual quality in different areas ranged from 7.95% to 12.45%, which verified the validity of the established simulation model in simulating the extrusion process of rice straw powder.

3) The results of the rice straw powder extrusion simulation tests show that the screw configuration has a direct effect on the filling degree of different regions. There is a highly significant correlation between the filling degree and other parameters, making it a crucial indicator of the changes in the state of motion during the rice straw extrusion process. The kneading region has the highest degree of filling and increases the degree of filling in the front conveying region by 33.94%. With the increase of filling degree, the average retention time of particles in the kneading element

region increases by 0.97 seconds compared to the conveying region. In addition, the kneading element exerts a shear force on the particles only in the tangential direction and is periodic in nature. This periodic force exerted to produce local pressure difference, which is the kneading element of the material with axial transport role of the fundamental reason.

4) The results of the extrusion comparison test of rice straw powder under different screw configurations show that there is a highly significant linear correlation between the simulated power consumption and the actual power consumption as well as the average particle size of the samples. It proves that the simulation model of rice straw powder extrusion established in this study has certain practical application value in guiding the design of different screw configurations.

Acknowledgements

This study was supported by the National Key R&D Program of China (Grant No. 2022YFD2002001), the Hunan Province Science and Technology Major Project (Grant No. 2023NK1020), the Hunan Province Graduate Research Innovation (Grant No. CX20230691), the Natural Science Foundation of Hunan Province (Grant No. 2022JJ40166), and the Scientific Research Project of the Hunan Provincial Department of Education (Grant No. 23B0197).

[References]

[1] Wang F, Liu X F, Chen L G, Lei T Z, Yi W M, Li Z H. Research status and development prospect of energy and high value utilization of biomass resources. Transactions of the CSAE, 2021; 37(18): 219–231. (in Chinese)

[2] Ahmed S F, Rafa N, Mofijur M, Badruddin I A, Inayat A, Ali M S, et al. Biohydrogen production from biomass sources: Metabolic pathways and economic analysis. Frontiers in Energy Research, 2021; 9: 753878.

[3] Sharma R, Singhal S, Tiwari A K, Agarwal S, Arora S, Singhal N. Influence of pretreatment processes onto bio-methanation of wheat straw. Journal of Renewable and Sustainable Energy, 2015; 7(5): 053109.

[4] Hsu T-C, Guo G-L, Chen W-H, Hwang W-S. Effect of dilute acid pretreatment of rice straw on structural properties and enzymatic hydrolysis. Bioresource Technology, 2010; 101(13): 4907–4913.

[5] Shen F, Xiong X, Fu J, Yang J, Qiu M, Qi X, Tsang D C W. Recent advances in mechanochemical production of chemicals and carbon materials from sustainable biomass resources. Renewable and Sustainable Energy Reviews, 2020; 1305: 109944.

[6] Pérez-Merchán A M, Rodríguez-Carballo G, Torres-Olea B, García-Sancho C, Maireles-Torres P J, Mérida-Robles J, et al. Recent advances in mechanochemical pretreatment of lignocellulosic biomass. Energies, 2022; 15(16): 5948.

[7] Zheng J, Choo K, Rehmann L. Xylose removal from lignocellulosic biomass via a twin-screw extruder: The effects of screw configurations and operating conditions. Biomass and Bioenergy, 2016; 88: 10–16.

[8] Geng X Z. Twin screw extruders and their applications. Beijing: China Light Industry Press. 2003; 466.

[9] Elalami D, Aouine M, Monlau F, Guillon F, Dumon C, Hernandez Raquet G, et al. Enhanced enzymatic hydrolysis of corn stover using twin - screw extrusion under mild conditions. Biofuels, Bioproducts and Biorefining, 2022; 16(6): 1642–1654.

[10] Yağcı S, Sutay Kocabaş D, Çalışkan R, Özbek H N. Statistical investigation of the bioprocess conditions of alkali combined twin - screw extrusion pretreatment to enhance fractionation and enzymatic hydrolysis of bulgur bran. Journal of the Science of Food and Agriculture, 2022; 102(11): 4770–4779.

[11] Morales-Huerta J C, Hernández-Meléndez O, Hernández-Luna M G, Manero O, Bárzana E, Vivaldo-Lima E. An experimental and modeling study on the pretreatment and alkaline hydrolysis of blue agave bagasse in twin-screw extruders. Industrial & Engineering Chemistry Research, 2021; 60(34): 12449–12460.

[12] Gu B-J, Dhumal G S, Wolcott M P, Ganjyal G M. Disruption of lignocellulosic biomass along the length of the screws with different screw elements in a twin-screw extruder. Bioresource Technology, 2019; 275: 266–271.

[13] Meier R, Moll K-P, Krumme M, Kleinebudde P. Impact of fill-level in twin-screw granulation on critical quality attributes of granules and tablets. European Journal of Pharmaceutics and Biopharmaceutics, 2017; 115: 102–112.

[14] Mundozah A L, Cartwright J J, Tridon C C, Hounslow M J, Salman A D. Hydrophobic/hydrophilic powders: Practical implications of screw element type on the reduction of fines in twin screw granulation. Powder Technology, 2019; 341: 94–103.

[15] Li A Q, Jia F G, Han Y L, Chen P Y, Wang Y L, Zhang J C, et al. Study on dynamic response mechanism of rice grains in friction rice mill and scale-up approach of parameter based on discrete element method. Innovative Food Science & Emerging Technologies, 2023; 86: 103346.

[16] Havlica J, Jirounkova K, Travnickova T, Kohout M. The effect of rotational speed on granular flow in a vertical bladed mixer. Powder Technology, 2015; 280: 180–190.

[17] Li A Q, Jia F G, Wang Y L, Han Y L, Chen P Y, Zhang J C, et al. Numerical analysis of the rice transport uniformity in vertical friction rice mill based on discrete element method. Computers and Electronics in Agriculture, 2022; 202: 107398.

[18] Li X, Hou Q F, Dong K J, Zou R P, Yu A B. Promote cohesive solid flow in a screw feeder with new screw designs. Powder Technology, 2020; 361: 248–257.

[19] Zheng C, Govender N, Zhang L, Wu C-Y. GPU-enhanced dem analysis of flow behaviour of irregularly shaped particles in a full-scale twin screw granulator. Particuology, 2022; 61: 30–40.

[20] Cheng H T, Gong Y J, Zhao N, Zhang L J, Lv D Q, Ren D Z. Simulation and experimental validation on the effect of twin-screw pulping technology upon straw pulping performance based on tavares mathematical model. Processes, 2022; 10(11): 2336.

[21] Rol F, Vergnes B, El Kissi N, Bras J. Nanocellulose production by twin-screw extrusion: simulation of the screw profile to increase the productivity. ACS Sustainable Chemistry & Engineering, 2020; 8(1): 50–59.

[22] Wang W W, Cai D Y, Xie J J, Zhang C L, Liu L C, Chen L Q. Calibration of discrete element model parameters for corn stover powder dense molding. Transactions of the CSAM, 2021; 52(3): 127–134. (in Chinese)

[23] Li Y X, Li F X, Xu X M, Shen C P, Meng K P, Chen J, et al. Calibration of discrete element parameters for wheat flour based on particle scaling. Transactions of the CSAE, 2019; 35(16): 320–327. (in Chinese)

[24] Horabik J, Molenda M. Parameters and contact models for dem simulations of agricultural granular materials: A review. Biosystems Engineering, 2016; 147: 206–225.

[25] Zheng C, Zhang L, Govender N, Wu C-Y. DEM analysis of residence time distribution during twin screw granulation. Powder Technology, 2021; 377: 924–938.

[26] Konan D, Koffi E, Ndao A, Peterson E C, Rodrigue D, Adjallé K. An overview of extrusion as a pretreatment method of lignocellulosic biomass. Energies, 2022; 15(9): 3002.

[27] Said N, Abdel daiem M M, García-Maraver A, Zamorano M. Influence of densification parameters on quality properties of rice straw pellets. Fuel Processing Technology, 2015; 138: 56–64.

[28] Chan Seem T, Rowson N A, Gabbott I, de Matas M, Reynolds G K, Ingram A. Asymmetric distribution in twin screw granulation. European Journal of Pharmaceutics and Biopharmaceutics, 2016; 106: 50–58.

[29] Chen X H, Zhang Y L, Gu Y, Liu Z G, Shen Z, Chu H Q, et al. Enhancing methane production from rice straw by extrusion pretreatment. Applied Energy, 2014; 122: 34–41.

[30] Zhang L, Lu H, Yu J, Wang Z, Fan Y, Zhou X. Dissolution of lignocelluloses with a high lignin content in a *N* -Methylmorpholine- *N* -Oxide monohydrate solvent system via simple glycerol-swelling and mechanical pretreatments. Journal of Agricultural and Food Chemistry, 2017; 65(44): 9587–9594.

[31] Matsushita M, Ohsaki S, Nara S, Nakamura H, Watano S. Effect of fill level in continuous twin-screw granulator: A combined experimental and simulation study. Advanced Powder Technology, 2022; 33(11): 103822.

[32] Xu B P, Liang R F, Xiao S P, Feng Y H, Yu H W. Improving mixing by changing topology through intermeshed perturbation rings in a co - rotating non - twin screw channel. Macromolecular Theory and Simulations, 2024; 33(2): 2300048.

[33] Yacu W. Extruder screw, barrel, and die assembly: General design principles and operation. In: Ganjyal G M. (Ed.). Extrusion Cooking. Woodhead Publ. & Cereals & Grains Assoc. Bookstore. 2020; pp.73–117. doi: 10.1016/B978-0-12-815360-4.00003-1.